

Fermi-surface-dependent superconducting gap in C_6Ca

K. Sugawara¹, T. Sato^{1*} and T. Takahashi^{1,2}

The discovery of superconductivity in C_6Yb and C_6Ca (ref. 1) has activated fierce debates on whether it is described within the conventional Bardeen–Cooper–Schrieffer scheme or some other exotic mechanisms are involved, because the superconducting transition temperature (T_c) is significantly higher than that of the alkali-metal graphite intercalation compounds intensively studied in the 1980s (refs 2–4). The key to understand the mechanism of superconductivity lies in the superconducting energy gap associated with the formation of superconducting pairs. Here, we report the first direct observation of a superconducting gap in C_6Ca by high-resolution angle-resolved photoemission spectroscopy. We found that the superconducting gap of 1.8–2.0 meV opens on the intercalant Fermi surface, whereas the gap is very small or absent on the Fermi surface derived from the π^* band of graphene layers. These experimental results unambiguously establish that the interlayer band has an essential role for the high- T_c superconductivity in C_6Ca .

Although the thermodynamic⁵ and magnetic properties⁶ of C_6Ca infer the isotropic *s*-wave superconducting order parameter within the conventional Bardeen–Cooper–Schrieffer theory, substantial deviations and anomalies beyond the conventional framework have been reported by tunnelling spectroscopy^{7,8} and electron spin resonance experiments⁹, proposing the strong-coupling superconductivity, the anisotropic gap and/or the multi-component gaps. The discovery of ‘high- T_c ’ graphite intercalation compounds has stimulated several theoretical proposals for the superconducting mechanism, ranging from the electronic pairing¹⁰ to the coupling to lattice vibrations (phonons)^{11–15}. Recent first-principles calculations^{11–15} have suggested that the electron coupling to the out-of-plane carbon and intercalant phonons is responsible for achieving higher T_c values, although a clear demonstration to experimentally distinguish various models has not yet been made. This key issue as well as the discrepancy in the nature of the superconducting gap among experiments urgently requires further precise investigations on the momentum and Fermi-surface dependence of the superconducting gap. Although angle-resolved photoemission spectroscopy (ARPES) is most suitable for these investigations, few such experiments have been carried out because of the small superconducting gap as well as the lack of high-quality single crystals. We used a high-quality C_6Ca single crystal grown from kish graphite (artificially grown single-crystalline graphite). We have succeeded for the first time in observing the interlayer band and the Fermi-surface-sheet-dependent superconducting gap and electron–phonon coupling.

Figure 1 shows the temperature dependence of the magnetic susceptibility of the C_6Ca sample for zero field cooling and field

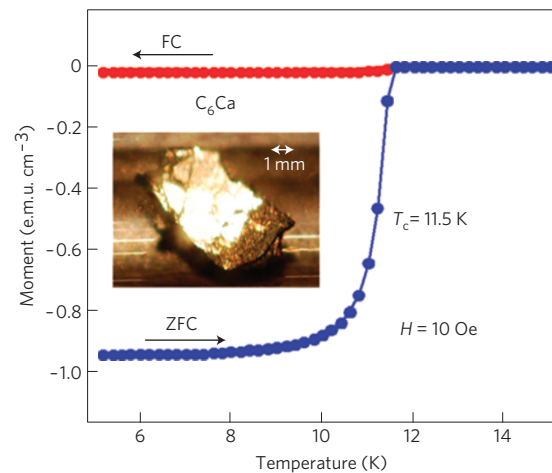


Figure 1 | Characterization of C_6Ca single crystal. Magnetic susceptibility of C_6Ca as a function of temperature for zero field cooling (ZFC) and field cooling (FC) at 10 Oe. Inset: Photograph of a C_6Ca single crystal used for ARPES measurements.

cooling at 10 Oe. The sharp drop in the zero-field-cooling curve confirms that the crystal exhibits superconductivity with the onset $T_c = 11.5$ K.

Figure 2a,b shows the experimentally determined valence-band structure along two high-symmetry lines ΓK and ΓM . Although the overall band structure looks similar between graphite and C_6Ca , the band dispersion of C_6Ca is shifted as a whole towards high binding energy by 1.0–1.5 eV, indicating that electrons are certainly doped into pristine graphite by Ca intercalation. A small electron pocket that appears near the Fermi level (E_F) at the K point in C_6Ca is ascribed to the $C 2p\pi^*$ band, which is above E_F in pristine graphite and is shifted down below E_F by electron doping^{16–18}. It is noted that the overall valence-band dispersion basically follows the periodicity of the Brillouin zone for graphite rather than that for C_6Ca , possibly owing to the relatively weaker periodic potential of C_6Ca with the $R\bar{3}m$ symmetry than the potential of bulk graphite. Figure 2c shows the Fermi surface of C_6Ca determined by ARPES, compared with that of graphite (Fig. 2d). The Fermi-surface topology of C_6Ca is drastically different from that of graphite. In C_6Ca , we find two different Fermi surfaces, a circular Fermi surface at the Γ point and a triangular Fermi surface at the K point, whereas only one tiny Fermi surface is observed at the K(H) point in graphite¹⁹. The triangular Fermi surface at the K point originates in the π^* band and is well explained in terms of the simple rigid shift of the chemical potential due to the

¹Department of Physics, Tohoku University, Sendai 980-8578, Japan, ²WPI Research Center, Advanced Institute for Material Research, Tohoku University, Sendai 980-8577, Japan. *e-mail: t-sato@arpes.phys.tohoku.ac.jp.

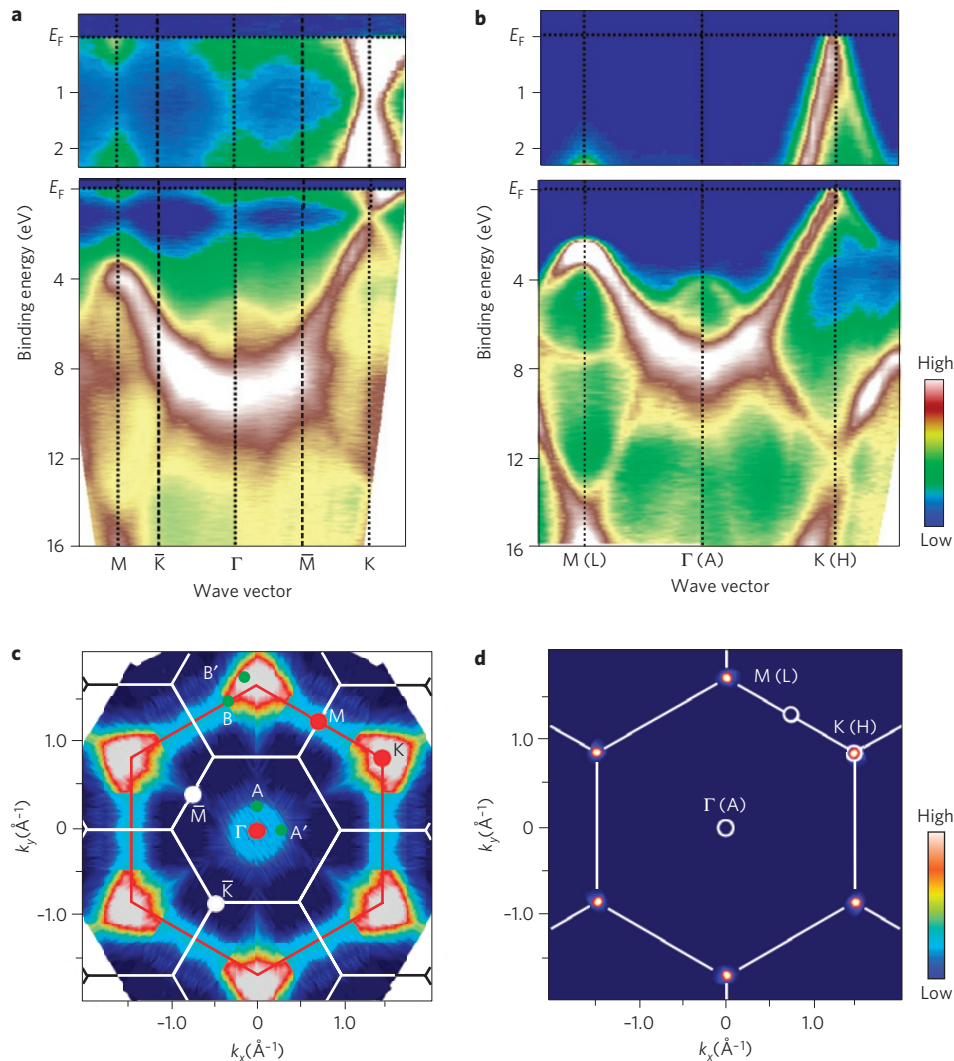


Figure 2 | Comparison of electronic structure and Fermi surface between C_6Ca and graphite. **a, b**, Valence-band structure of C_6Ca (**a**) and graphite (**b**), determined by plotting the ARPES spectral intensity as a function of wave vector and binding energy. Expansion near E_F is also shown in the upper panel. **c, d**, Fermi surfaces for C_6Ca (**c**) and graphite (**d**), determined by plotting the ARPES spectral intensity integrated within ± 10 meV with respect to E_F and folding with the hexagonal symmetry. Solid red and white lines in **c** are surface Brillouin zones of graphene and C_6Ca , respectively.

electron doping²⁰. In contrast, the small Fermi surface observed at the Γ point is not explained by the simple rigid shift of graphite bands or the folding of the π^* band due to the superstructure of Ca intercalants, because the shape and size of the Fermi surface are distinctly different from those of the π^* Fermi surface. On the other hand, the band-structure calculations^{10–15} have predicted an extra band at the Γ point in C_6Ca named the interlayer band, which has a sizable contribution from the intercalant states and produces a small free-electron-like spherical Fermi surface at the Γ point. Considering a good agreement in the location and the shape as well as the superconducting-gap size (discussed later in detail), we assign the small Fermi surface observed at the Γ point to the interlayer band in C_6Ca . To our best knowledge, this is the first direct observation of the interlayer band in graphite intercalation compounds.

Figure 3a shows ARPES spectra near E_F of C_6Ca at 6 K measured at two representative Fermi vectors (k_F) on the circular Fermi surface at the Γ point and the triangular Fermi surface at the K point, respectively. The spectral intensity shows a sudden drop at 80 meV on the circular Fermi surface (point A), whereas a small but clear dip is observed at 170 meV in the spectrum measured

on the triangular Fermi surface (point B). The energy position of the 170 meV dip is similar to that of the dispersion kink observed in graphite²¹ and C_6Ca (ref. 22). We find that the energy position of the dip does not vary in the momentum region around the k_F point. This is not explained by the presence of another band located around the dip energy, but is reminiscent of the strong many-body effects observed in high- T_c copper oxides^{23,24} and $Ba_{0.67}K_{0.33}BiO_3$ (ref. 25). In fact, as seen in Fig. 3a, the Eliashberg function $\alpha^2F(\omega)$ calculated for C_6Ca (ref. 11) shows dominant peaks at 50–75 meV and 160–180 meV originating in the out-of-plane and the in-plane vibrations of carbon atoms, respectively, in good agreement with the anomalies in the ARPES spectra. This suggests that electrons on the circular Fermi surface at the Γ point are strongly coupled to the out-of-plane vibrations, whereas those on the triangular Fermi surface at the K point are coupled dominantly with the in-plane phonons. This experimentally demonstrates that the interlayer electrons strongly interact with the surrounding lattice unlike in the free-electron picture, as predicted from first-principles calculations^{13,14}. The reason π^* electrons at the K point are only weakly coupled to the out-of-plane phonons may be the antisymmetry of the wave function with respect to

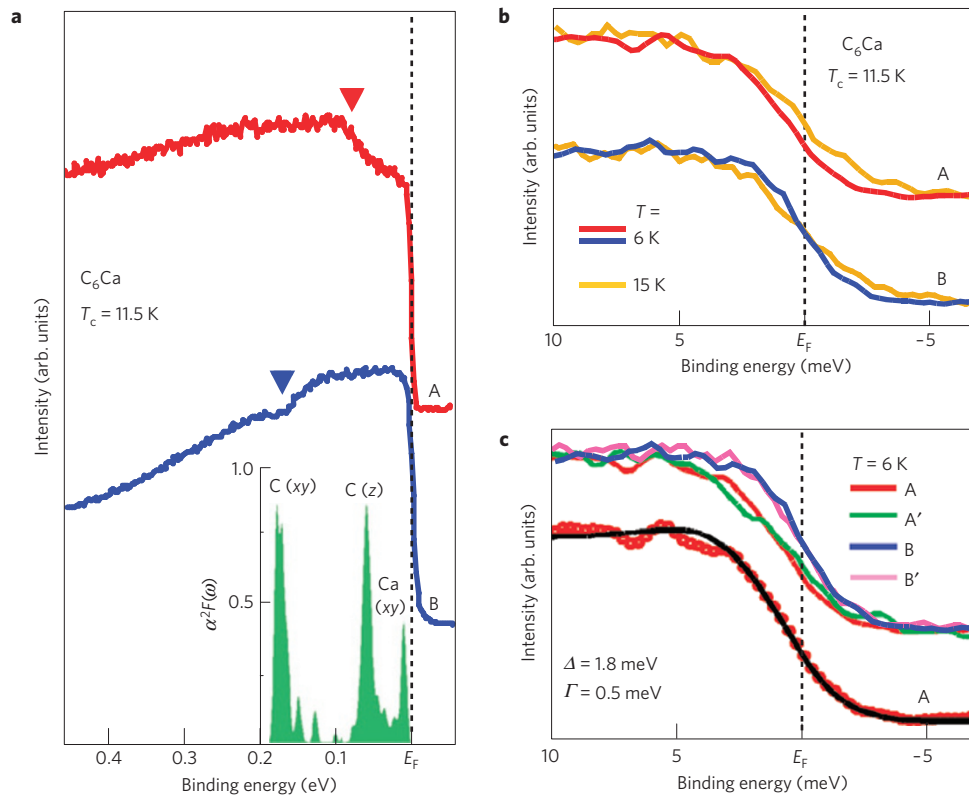


Figure 3 | Electron-phonon coupling and superconducting gap in C_6Ca . **a**, ARPES spectra of C_6Ca measured at 6 K on (A) the circular Fermi surface and (B) the triangular Fermi surface (points A and B in Fig. 2c, respectively), compared with the calculated Eliashberg function $\alpha^2F(\omega)$ as a function of binding energy¹¹. Filled triangles denote the characteristic energy scales where the spectrum shows a distinct anomaly. **b**, ARPES spectra of C_6Ca in the vicinity of E_F at points A and B, measured at temperatures below/above T_c (6 K and 15 K). **c**, Top: Comparison of ARPES spectrum at 6 K among points A, A', B and B'. Bottom: Numerical fit (black curve) to the 6 K spectrum at point A (red circles) with the Dynes function²⁶ multiplied by the Fermi-Dirac function at $T = 6$ K convoluted with a Gaussian taking into account the instrumental resolution.

the graphene layer¹¹. On the other hand, the interlayer band forming the circular Fermi surface at the Γ point is expected to be strongly coupled to the out-of-plane phonons owing to the symmetry¹⁴. A spectral dip related to the coupling with the Ca vibrations is not clearly observed in Fig. 3a, possibly because the dip is broad (20–30 meV) compared with the Ca phonon energy (15 meV).

Figure 3b shows ultrahigh-resolution ARPES spectra near E_F of C_6Ca measured at the same two points as in Fig. 3a at temperatures below/above T_c . At point A, the midpoint of the leading edge in the spectrum at 6 K is shifted towards high binding energy by approximately 0.8 meV with respect to E_F , whereas the spectrum at 15 K has the midpoint at E_F . This clearly indicates the opening/closing of a superconducting gap as a function of temperature. On the other hand, at point B, the midpoint of the leading edge is located at around E_F even at 6 K, and the spectrum shows a simple temperature dependence to obey the Fermi-Dirac function, suggesting the absence or the very small magnitude of the superconducting gap. This marked difference is better illustrated in Fig. 3c, where the spectra at 6 K at points A and B are directly compared. To clarify the possible anisotropy of the gap in each Fermi-surface sheet, we also plot the 6 K spectra measured at points A' and B' on the same Fermi surfaces but on different high symmetry lines (Fig. 2c), because the anisotropy, if it exists, should be largest between points A and A' (B and B'). We note that the ARPES technique basically observes the gap averaged over k_z (k perpendicular to the surface), so that it measures the anisotropy of the gap in the k_x - k_y plane. As seen from Fig. 3c, the leading edge at point A' (B') almost coincides

with that of point A (B). This suggests that the anisotropy of the superconducting gap is very small in both circular and triangular Fermi surfaces, although the gap size is markedly different between these two Fermi surfaces. To estimate the size of the superconducting gap, we numerically fit the spectrum using the Dynes function²⁶. The representative result for point A is shown in Fig. 3c. The estimated gap size Δ at 6 K is 1.8 ± 0.2 and 2.0 ± 0.2 meV at points A and A', respectively. The reduced gap value of $2\Delta(0)/k_B T_c$ determined by assuming the mean-field temperature dependence is 4.1 ± 0.5 , indicating intermediate- to strong-coupling character. The first-principles calculation¹³ has predicted a similar gap value. On the other hand, at points B and B', the estimated superconducting-gap size is 0.2 ± 0.2 meV. These results suggest that the deviation from the single isotropic s -wave gap function in the tunnelling density of states⁷, interpreted in terms of the anisotropic s -wave gap, is not explained by the anisotropy of the gap within the interlayer Fermi surface at the Γ point, but is actually influenced by a smaller superconducting gap of other Fermi surfaces, most likely the π^* Fermi surface. The reported deviation of the specific heat²⁷ from the single isotropic s -wave behaviour^{13,15} would also be explained by this Fermi-surface dependence of the superconducting gap.

The present results demonstrate that the coupling of electrons in the interlayer band with the out-of-plane phonons is essential to realize superconductivity in C_6Ca , whereas simple electron doping into the π^* band of graphene layers may not lead to superconductivity at such a high temperature. The next challenge is to clarify the role of intercalant (Ca) phonons, which have been theoretically proposed to enhance the T_c value^{11–15}.

Methods

High-quality C_6Ca single crystals were grown by heating kish graphite mixed with molten lithium–calcium alloy at around 350 °C for 6 days under high vacuum²⁸. The typical size of the crystals was $3 \times 3 \times 0.5 \text{ mm}^3$. ARPES measurements were carried out using an SES-2002 spectrometer with a high-flux discharge lamp and a toroidal grating monochromator at Tohoku University. As the sample is very unstable in the atmosphere, almost all of the steps such as sample mounting were done in a glove box filled with Ar gas. The superconducting volume fraction is estimated to be $90 \pm 10\%$ at 5 K, higher than previous reports^{1,28}. The X-ray diffraction measurement confirmed that inclusion of C_6Li is at most 5%. The crystal was cleaved *in situ* along the (0001) plane in an ultrahigh vacuum better than 2×10^{-11} torr to obtain a clean surface for ARPES measurements. The He II α (40.814 eV) resonance line was used to excite photoelectrons. The energy and angular (momentum) resolutions were set at 4.5 meV and 0.2° (0.01 \AA^{-1}), except for in the measurement of the wide valence-band region ($\Delta E = 16 \text{ meV}$). The temperature of the samples was controlled to remain stationary within $\pm 0.1 \text{ K}$ during measurements by monitoring with a silicon diode sensor embedded below the sample. The Fermi level of the sample was referenced to that of a gold film deposited onto the sample substrate. No degradation of the sample surface was observed during the measurements. We checked the reproducibility of the data by measuring several samples.

Received 8 April 2008; accepted 8 October 2008;
published online 9 November 2008

References

- Weller, T. E., Ellerby, M., Saxena, S. S., Smith, R. P. & Skipper, N. T. Superconductivity in the intercalated graphite compounds C_6Yb and C_6Ca . *Nature Phys.* **1**, 39–41 (2005).
- Dresselhaus, M. S. & Dresselhaus, G. Intercalation compounds of graphite. *Adv. Phys.* **51**, 1–186 (2002).
- Hannay, N. B. *et al.* Superconductivity in graphitic compounds. *Phys. Rev. Lett.* **14**, 225–226 (1965).
- Belash, I. T., Bronnikov, A. D., Zharikov, O. V. & Palnichenko, A. V. On the superconductivity of graphite intercalation compounds with sodium. *Solid State Commun.* **64**, 1445–1447 (1987).
- Sutherland, M. *et al.* Bulk evidence for single-gap s-wave superconductivity in the intercalated graphite superconductor C_6Yb . *Phys. Rev. Lett.* **98**, 067003 (2007).
- Lamura, G. *et al.* Experimental evidence of s-wave superconductivity in bulk C_6Ca . *Phys. Rev. Lett.* **96**, 107008 (2006).
- Bergeal, N. *et al.* Scanning tunnelling spectroscopy on the novel superconductor C_6Ca . *Phys. Rev. Lett.* **97**, 077003 (2006).
- Kürter, C. *et al.* Large energy gaps in C_6Ca from tunnelling spectroscopy: Possible evidence of strong-coupling superconductivity. *Phys. Rev. B* **76**, 220502(R) (2007).
- Murànu, F., Urbanik, G., Kataev, V. & Büchner, B. Electron spin dynamics of the superconductor C_6Ca probed by ESR. *Phys. Rev. B* **77**, 024507 (2008).
- Csanyi, G. *et al.* The role of the interlayer state in the electronic structure of superconducting graphite intercalated compounds. *Nature Phys.* **1**, 42–45 (2005).
- Calandra, M. & Mauri, F. Theoretical explanation of superconductivity in C_6Ca . *Phys. Rev. Lett.* **95**, 237002 (2005).
- Mazin, I. I. Intercalant-driven superconductivity in YbC_6 and C_6Ca . *Phys. Rev. Lett.* **95**, 227001 (2005).
- Sanna, A. *et al.* Anisotropic gap of superconducting C_6Ca : A first-principles density functional calculation. *Phys. Rev. B* **75**, 020511(R) (2007).
- Boeri, L. *et al.* Electron–phonon interaction in graphite intercalation compounds. *Phys. Rev. B* **76**, 064510 (2007).
- Mazin, I. I. *et al.* Unresolved problems in superconductivity of C_6Ca . *Physica C* **460–462**, 116–120 (2007).
- Takahashi, T. *et al.* Electronic band structure of C_8K studied by angle-resolved ultraviolet photoelectron spectroscopy. *J. Phys. Soc. Jpn* **55**, 3498–3502 (1986).
- Molodtsov, S. L. *et al.* Folded bands in photoemission spectra of La-graphite intercalation compounds. *Phys. Rev. B* **67**, 115105 (2003).
- McChesney, J. L. *et al.* Massive enhancement of electron–phonon coupling in doped graphene by an electronic singularity. Preprint at <<http://arxiv.org/abs/0705.3264>> (2007).
- Sugawara, K. *et al.* Fermi surface and edge-localized states in graphite studied by high-resolution angle-resolved photoemission spectroscopy. *Phys. Rev. B* **73**, 045124 (2006).
- Tatar, R. C. & Rabii, S. Electronic properties of graphite: A unified theoretical study. *Phys. Rev. B* **25**, 4126–4141 (1982).
- Sugawara, K. *et al.* Anomalous quasiparticle lifetime and strong electron–phonon coupling in graphite. *Phys. Rev. Lett.* **98**, 036801 (2007).
- Valla, T. *et al.* Anisotropic electron–phonon coupling and dynamical nesting on the graphene sheets in C_6Ca . Preprint at <<http://arxiv.org/abs/0803.0254>> (2008).
- Damascelli, A., Hussain, Z. & Shen, Z.-X. Angle-resolved photoemission studies of the cuprate superconductors. *Rev. Mod. Phys.* **75**, 473–541 (2003).
- Campuzano, J. C., Norman, M. R. & Randeria, M. in *Physics of Conventional and Unconventional Superconductors* Vol. 2 (eds Bennemann, K. H. & Ketterson, J. B.) 167–273 (Springer, 2004).
- Chainani, A. *et al.* Electron–phonon coupling induced pseudogap and the superconducting transition in $Ba_{0.67}K_{0.33}BiO_3$. *Phys. Rev. B* **64**, 180509(R) (2001).
- Dynes, R. C., Narayanamurti, V. & Garno, J. P. Direct measurement of quasiparticle-lifetime broadening in a strong-coupled superconductor. *Phys. Rev. Lett.* **41**, 1509–1512 (1978).
- Kim, J. S., Kremer, R. K., Boeri, L. & Razavi, F. S. Specific heat of the Ca-intercalated superconductor C_6Ca . *Phys. Rev. Lett.* **96**, 217002 (2006).
- Emery, N. *et al.* Superconductivity of bulk C_6Ca . *Phys. Rev. Lett.* **95**, 087003 (2005).

Acknowledgements

We thank H. Suematsu for providing high-quality kish graphite. We also thank K. Tanigaki, K. Sato, T. Rachi and K. Kadowaki for their help in the sample preparation. This work was supported by grants from JSPS, JST-CREST and MEXT of Japan.

Author contributions

K.S. and T.S. shared responsibility for all aspects of this project including instrument construction, data collection, analysis and sample growth. T.T. contributed to the project planning and managed the whole project.

Additional information

Reprints and permissions information is available online at <http://npg.nature.com/reprintsandpermissions>. Correspondence and requests for materials should be addressed to T.S.